Heliyon 10 (2024) e23371

Contents lists available at ScienceDirect

Heliyon

journal homepage: www.cell.com/heliyon

Amino acid promoted oxidation of atrazine by Fe_3O_4/persulfate

Mingming Zheng [a,1], Yinghao Li [b,1], Menghua Cao [b,*], Yuxin Guo [b], Guohong Qiu [b], Shuxin Tu [b], Shuanglian Xiong [b], Dun Fang [c]

[a] School of Chemical and Environmental Engineering, Wuhan Polytechnic University, Wuhan, 430023, PR China
[b] Hubei Key Laboratory of Soil Environment and Pollution Remediation, College of Resources and Environment, Huazhong Agricultural University, Wuhan 430070, PR China
[c] School of Chemistry and Environmental Engineering, Hubei Minzu University, Enshi, 445000, PR China

ARTICLE INFO

Keywords:
Cysteine
Magnetite
Iron cycle
Persulfate
Atrazine

ABSTRACT

In the present study, we demonstrated that the presence of cysteine could remarkably enhance the degradation of atrazine by Fe_3O_4/persulfate system. The results of electron paramagnetic resonance (EPR) spectra confirmed the combination of cysteine and Fe_3O_4 exhibited much higher activity on activation of persulfate to generate more $SO_4^{\bullet-}$ and •OH than Fe_3O_4 alone. At pH of 3.0, $SO_4^{\bullet-}$ and •OH contributed to about 58.2 % and 41.8 % of atrazine removal respectively, while •OH gradually dominated the oxidation of atrazine from neutral condition to alkaline condition. The co-existing Cl^- and HCO_3^- could quench $SO_4^{\bullet-}$, resulting in the inhibition of atrazine degradation. The presence of low natural organic matters (NOM) concentration (0–2 mg L^{-1}) could enhance the atrazine removal, and high concentration (>5 mg L^{-1}) of NOM restrained the atrazine degradation. During the Cysteine/Fe_3O_4/Persulfate process, cysteine served as a complexing reagent and reductant. Through acidolysis and complexation, Fe_3O_4 could release dissolved and surface bound Fe^{2+}, both of which contributed to the activation of persulfate together. Meanwhile, cysteine was not rapidly consumed due to a regeneration process, which was beneficial for maintaining Fe^{2+}/Fe^{3+} cycle and constantly accelerating the activation of persulfate for atrazine degradation. The reused Fe_3O_4 and cysteine in the Cysteine/Fe_3O_4/Persulfate process exhibited high stability for the atrazine degradation after three cycles. The degradation pathway of atrazine included alkylic-oxidation, dealkylation, dechlorination-hydroxylation processes. The present study indicates the novel Cysteine/Fe_3O_4/Persulfate process might be a high potential for treatment of organic polluted water.

1. Introduction

Atrazine is one of effective triazine herbicides widely utilized for broadleaf weed control [1,2]. Due to the limited absorption at wavelengths over 220 nm, photolysis of atrazine by sunlight occurs slowly, making it difficult for microorganisms to breakdown [3]. As a result, atrazine is a refractory and persistent organic pollutant with a half-life of 41–231 d [4]. Atrazine could quickly migrate to deep layers of the soil and is transported to surface water or groundwater by surface runoff due to its high soil solubility. It has been

* Corresponding author.
E-mail addresses: zhengmm2008@126.com (M. Zheng), Liyinghao200204@163.com (Y. Li), caomenghua@mail.hzau.edu.cn (M. Cao), qiugh@mail.hzau.edu.cn (G. Qiu), stu@mail.hzau.edu.cn (S. Tu), xsl@mail.hzau.edu.cn (S. Xiong), fangdun2008@163.com (D. Fang).
[1] These authors contributed equally to this work.

https://doi.org/10.1016/j.heliyon.2023.e23371
Received 22 November 2023; Accepted 1 December 2023
Available online 6 December 2023

prohibited from use in EU member states since 2003 as a typical organic compound with high carcinogenic potential because it was listed as a group 3 carcinogen by the WHO in 2017 [5]. Although it is currently legal to use in China and the USA, it is regularly found in groundwater and surface waters, endangering human health through consumption of tainted water. Investigating environmentally friendly ways to clean up atrazine-contaminated water is crucial for ensuring human health.

In the recent years, the advanced oxidants processes (AOPs) have been widely used to remediate organic polluted water due to its outstanding degradation and mineralization efficiency [6–9]. Among AOPs, persulfate oxidation technology has drawn a lot of interest due to its strong oxidizing capacity and room temperature stability. Sulfate radicals ($SO_4^{\bullet-}$) could be produced with the activation of persulfate as a result of the catalysis of UV light, heat, base, materials containing transition metals, carbon, and quinones [10–15]. Subsequently, $SO_4^{\bullet-}$ can reactive with water to produce hydroxyl radicals (•OH). As a result, these reactive oxidants can break down the persistent organic contaminants. Among these catalysts, irons-contained materials attracted the most attention due to their widespread availability, affordable treatment, and environmentally friendly properties. For example, $FeSO_4$ is one the most common agent to activate persulfate [16,17]. However, the degradation efficiency is limited by the high consumption of Fe^{2+} and the accumulation of iron sludge [18]. In order to solve this problem, iron minerals such as pyrite, hematite, goethite, and magnetite were employed as the heterogeneous activator to induce persulfate. In order to enhance the activation of persulfate by iron minerals, Fe-based metal organic frameworks (MOFs) were synthesized to increase the active sites [19,20]. Unfortunately, the majority of these iron minerals exhibit poor persulfate activation capability was due to insufficient Fe(II), which might be attributed to the difficulty in continuous Fe(II) release and a low transformation rate of Fe(III) to Fe(II) in the absence of electron donors [18,21,22]. Electrolytic manipulation and the addition of hydroxylamine were used to promote the transformation of Fe(III) to Fe(II) [23,24], which might involve the extra energy consumption or secondary pollution risk. Therefore, finding an affordable and environmentally benign agent that can enhance the recycling of Fe(III) and Fe(II) during the activation of persulfate with iron minerals is of utmost importance.

Cysteine, a type of necessary amino acid, is environmentally benign and pervasively found in many living cells of organisms, with a concentration of 200–300 μmol L^{-1} in animal blood [25]. It is commonly found in aquatic environments, where wastewater contains concentrations of up to 0.2 mg L^{-1} [26]. Cysteine is a naturally occurring reducing agent owing to the thiol group (-SH), which can speed up the reduction of Fe(III) to Fe(II) [27,28]. Meanwhile, the carboxyl group (-COOH) in cysteine molecules can be useful for the formation of Fe-complexes, which might be in favor of continuous Fe(II) release from iron minerals and reducing iron sludge. Therefore, the addition of cysteine might promote the degradation of atrazine by activation of persulfate with iron minerals. However, to our knowledge, the oxidation efficiency and mechanism of atrazine by cysteine/iron minerals/persulfate has been seldom reported.

In the recent study, we systematically investigated the degradation performance of atrazine by activation of persulfate with Fe_3O_4 and cysteine. Subsequently, the influencing factors including the dosage of different agents and the solution pH were explored in detail. Then, the contribution of cysteine on the transformation of Fe species and the generation of reactive oxygen species (ROSs) was discussed. Furthermore, the decomposition pathway of atrazine during the process was proposed. This study aims to deeply understand the promotion effects of cysteine on the activation of persulfate with iron minerals and develop new persulfate based environmental control and remediation technologies.

2. Materials and methods

2.1. Materials and chemicals

Atrazine (analytical grade) and cysteine (analytical grade) were purchased from Shanghai Yuanye Bio-Technology Company Limited (China). Fe_3O_4 (chemical grade), humic acid (analytical grade) and $AgNO_3$ (analytical grade) were offered by Shanghai Aladdin Biochemical Technology Company Limited (China). Persulfate sodium ($Na_2S_2O_8$, analytical grade) and *tert*-butyl alcohol (TBA, analytical grade) were bought from Sinopharm Chemical Reagent Company Limited (China). HPLC grade methanol and acetonitrile were supplied by Sigma-Aldrich (USA). Cysteine stock solution (10 mmol L^{-1}) and persulfate stock solution (100 mmol L^{-1}) were prepared by the deionized water. The atrazine solution (25 mg L^{-1}) was prepared by adding 0.05g atrazine to 1.6 L deionized water and being dissolved by a magnetic stirrer in the 40 °C water bath for 12 h, then filtered by 0.22 μm filter membrane and diluted the filtrate to the required concentration.

2.2. Experiments procedures

All of the oxidation experiments were conducted in a 100 mL conical glass flask containing 50 mL of atrazine (10 mg L^{-1}) at room temperature (25 ± 2 °C). A given mass of Fe_3O_4 and cysteine were added into the atrazine solution. Then, the pH values of the mixed solutions were adjusted by 0.1 mmol L^{-1} H_2SO_4 or NaOH. Subsequently, a given dosage of persulfate was added into the mixed solution to initiate the reaction. At the given time intervals, 0.5 mL of the suspension was withdrawn and filtered immediately through a polyethersulfone filter (0.22 μm) to remove the catalyst. The filtrate was promptly quenched with 1 mL ethanol before analysis. A series of experiments were carried out to investigate the impact of initial condition (cysteine, Fe_3O_4, persulfate, inorganic ions and natural organic matters (NOM) concentration, pH) on the degradation of atrazine. Humic acid is used to represent NOM. All experiments were carried out in triplicate with error bars in figures representing the standard deviation.

2.3. Chemical analysis

The concentration of atrazine was measured by high performance liquid chromatography (HPLC, Agilent 1260, USA), equipped

with an Agilent ZORBOX SB-C18 reversed phase column. The mobile phase for atrazine analysis was a mixture of acetonitrile and deionized water (volume ratio was 50:50). The wavelength of UV detector was kept in 220 nm. The mobile phase was performed at flow rate of 1.0 mL min^{-1}, while the column temperature was remained at 25 °C. The concentration of cysteine was also determined by HPLC (Agilent 1260, USA). The mobile phase contained 80 % of 0.1 % phosphoric acid and 20 % of acetonitrile, performed at flow rate of 0.6 ml min^{-1}. The wavelength of UV detector was maintained in 210 nm. The limit of detection values of the HPLC method for measuring the atrazine and cysteine was 10 μg L^{-1}. The atrazine degradation intermediates were analyzed by ultra-high performance liquid chromatography (Agilent 1290) and mass spectrometry (Agilent 6550 Q-TOF) with a chromatographic column (Waters, BEH C18, 2.1 mm × 100 mm × 1.7 μm). The eluants in liquid chromatography were deionized water (eluant A) and acetonitrile (eluant B). The flow rate was maintained at 0.3 ml min^{-1}. Alcohols quenching experiments with methanol and TBA were performed by adding the excess alcohols to the solution before the adjunction of Fe_3O_4. The methanol was used as a scavenger of the free radical •OH and $SO_4^{\bullet-}$, while *tert*-butyl alcohol (TBA) was applied as a scavenger of the free radical •OH [29]. The formation of •OH and $SO_4^{\bullet-}$ during the process were also analyzed by electron paramagnetic resonance spectra (EPR, EMCnano, Bruker, Germany), and 5,5-dimethyl-1-pyrroline-N-oxide (DMPO) was employed as the radical spin trapping reagent. The Fe_3O_4 was characterized by scanning electron microscopy (SEM, Zeiss Gemini 300, Zeiss, Germany), nanoparticle size potentiometer (NSP, Zetasize Nano ZS, UK) and X-ray powder diffraction (XRD, Bruker, Germany). SEM used Zeiss Gemini300 field emission electron microscope at a voltage of 5 kV. XRD was performed on a D8 ADVANCE with Cu Kα ration source generated at 40 KV and 20 mA. The Fe(II) concentration was measured by detecting the absorbance of Fe(II)-orthophenanthroline complex with a UV–Vis spectrophotometer (UV-2550, Shimadzu, Japan) at 510 nm. Hydroxylamine hydrochloride was used to convert Fe(III) to Fe(II), which was then subjected to the same analysis process as Fe(II) measurement in order to determine the total amount of dissolved iron. Meanwhile, Fe(III) concentration was determined by the difference between total irons and Fe(II). The persulfate concentration was quantified by KI colorimetric method [30].

3. Results and discussion

3.1. The degradation performance of atrazine in cysteine/Fe_3O_4/persulfate system

A series of preliminary experiments were run to compare the atrazine degradation in different systems. Fig. 1a showed the degradation efficiency of atrazine by Cysteine, Fe_3O_4, Persulfate, Cysteine/Fe_3O_4, Cysteine/Persulfate, Fe_3O_4/Persulfate and Cysteine/Fe_3O_4/Persulfate processes. These processes were carried out under the identical pH and the same dosage of persulfate, cysteine and Fe_3O_4. It could be observed negligible atrazine was removed in the Cysteine, Fe_3O_4 and Cysteine/Fe_3O_4 systems, which ruled out the reduction of cysteine and the adsorption of Fe_3O_4 on the removal of atrazine. Only 8.9 % of atrazine was removed by persulfate oxidation after 360 min. The addition of Fe_3O_4 could promote the degradation ratio of atrazine to 28.7 % by persulfate due to generation of $SO_4^{\bullet-}$ through the activation of persulfate with Fe_3O_4 [31], while cysteine had a little of inhibition on the degradation of atrazine by persulfate which might be due to the competitive oxidation between cysteine and atrazine. Fortunately, the co-occurrence of cysteine and Fe_3O_4 could significantly enhance the oxidation of atrazine by persulfate and the removal ratio reached 72.3 % after 360 min. Good correspondences with pseudo-first-order kinetics were employed to fit atrazine degradation rate in Fe_3O_4/Persulfate and Cysteine/Fe_3O_4/Persulfate systems (Fig. S1 in the Supplementary material (SM)). It could be observed the degradation of atrazine in Fe_3O_4/Persulfate involved two stages including the fast degradation within the initial 10 min (k_1 = 0.0217 min^{-1}) and the slow degradation in the remaining time (k_2 = 0.0004 min^{-1}). The degradation rate constant of atrazine in Cysteine/Fe_3O_4/Persulfate reached 0.0635 min^{-1} in the first stage, nearly 3 time that in Fe_3O_4/Persulfate system. Notably, atrazine still maintained high degradation rate (0.0025 min^{-1}) in Cysteine/Fe_3O_4/Persulfate during the second stage, which indicated cysteine might have the ability to continuously promote the degradation of atrazine by activating persulfate with Fe_3O_4. The dechlorination performances of atrazine were consistent with the degradation efficiency in the comparison systems, and dechlorination ratio in Persulfate, Cysteine/Persulfate, Fe_3O_4/Persulfate and Cysteine/Fe_3O_4/Persulfate achieved 4.32 %, 3.86 %, 7.85 % and 36.4 % respectively (the calculation of dechlorination ratio was defined in Text S1 in the SM) (Fig. 1b).

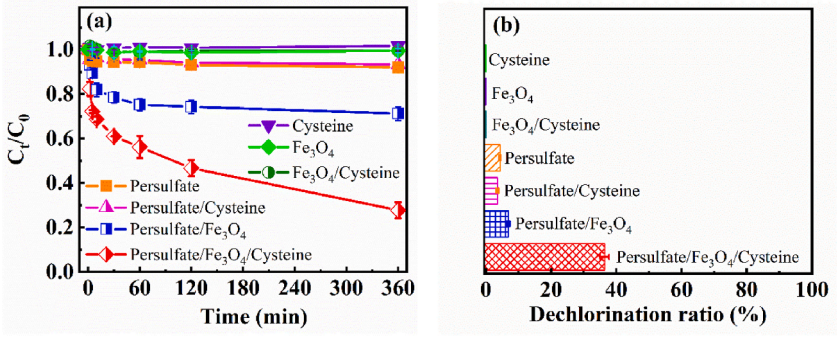

Fig. 1. Time profiles of atrazine degradation (a) and dichlorination ratio (b) in the comparison systems. (The initial condition: [Atrazine] = 10 mg L^{-1}, [Persulfate] = 1 mmol L^{-1}, [Cysteine] = 0.1 mmol L^{-1}, [Fe_3O_4] = 1 g L^{-1}, the initial pH was 3.0).

EPR spectra was explored to identify the generated ROSs in the Cysteine/Fe_3O_4/Persulfate system. Based on the hyperfine splitting constants, the mixture of cysteine, Fe_3O_4 and persulfate could induce the distinctive peak of DMPO-$SO_4^{\bullet-}$ ($a_N = 13.4$ G, $a_H = 9.5$ G, $a_H = 1.47$ G, $a_H = 0.76$ G) and DMPO-•OH ($a_N = a_H = 14.7$ G) (Fig. 2a) [12,15], indicating the production of $SO_4^{\bullet-}$ and •OH during the process. The generated •OH might originate from the reaction between $SO_4^{\bullet-}$ and OH^- [12]. Compared with EPR spectra of Fe_3O_4/-Persulfate, the presence of cysteine significantly promoted the peak intensities of DMPO-$SO_4^{\bullet-}$ and DMPO-•OH signals, revealing the addition of cysteine could dramatically raise the yield of ROSs in Fe_3O_4/Persulfate system. Meanwhile, much more consumption of persulfate was observed in Cysteine/Fe_3O_4/Persulfate than Fe_3O_4/Persulfate system (Fig. S2 in the SM), corresponding with the production of sulfate radicals. The contribution of ROSs on the degradation of atrazine by Cysteine/Fe_3O_4/Persulfate process was explored by radical scavenging experiments. Due to the high reaction rate constant with •OH ($k = 3.8–7.6 \times 10^8$) and slower reaction rate constant with $SO_4^{\bullet-}$ ($k = 4.0–9.1 \times 10^5$) [32], *tert*-butyl was performed as an effective scavenger for •OH. Meanwhile, owing to the high reaction rate constant with both •OH ($k = 9.7 \times 10^8$) and $SO_4^{\bullet-}$ ($k = 8.0 \times 10^7$) [3], methanol was utilized as a scavenger for •OH and $SO_4^{\bullet-}$. Chloroform and L-Histidine were the common scavengers for $O_2^{\bullet-}$ (3.0×10^9 M^{-1} s^{-1}) and $^1O_2$ (3.0×10^9 M^{-1} s^{-1}) respectively [33]. Fig. S3 (in the SM) showed 100 mmol L^{-1} methanol and tert-butanol were excess to capture the generated •OH and $SO_4^{\bullet-}$. With the addition of excess methanol and tert-butanol, the removal ratio of atrazine decreased from 67.9 % to 11.7 % and 39.5 % respectively, indicating both $SO_4^{\bullet-}$ and •OH contributed to the degradation of atrazine (Fig. 2b). At the same time, the removal ratio of atrazine decreased to 45.7 % and 52.6 % in the presence of excess chloroform and L-Histidine respectively, confirming $O_2^{\bullet-}$ and $^1O_2$ also participated in the degradation of atrazine.

To Further estimate the contribution of $^{\bullet}$OH, $SO_4^{\bullet-}$ and other active species on the degradation of atrazine, the competition kinetics experiment was conducted using the mixed system containing nitrobenzene (NB), benzoic acid (BA) and atrazine [34]. The degradation of NB, BA and atrazine and the steady-state concentration of $^{\bullet}$OH and $SO_4^{\bullet-}$ could be described as follows (Eqs. (1)–(5)) [34]. With the reported second-order rate

constants of radicals toward the NB, BA and atrazine (Table S1) and the experimental result (Fig. S4), the steady-state concentrations of •OH and $SO_4^{\bullet-}$ were calculated to be 5.32×10^{-14} and 2.31×10^{-13} mol/L respectively. Therefore, the relative contributions of •OH, $SO_4^{\bullet-}$, and other active species for the degradation of atrazine in the Cysteine/Fe_3O_4/Persulfate system were estimated to be 14.51 %, 63.24 % and 22.25 % respectively (Eqs. (6)–(8)) [34].

$$\ln\frac{[NB]}{[NB]_0} = -k_{(\cdot OH,NB)}[\cdot OH]_S t = -k_{(obs,NB}t \tag{1}$$

$$\mathrm{In}\frac{[BA]}{[BA]_0} = -\left(k_{(\bullet OH,BA)[OH]_s}\ k_{(SO_4^{\bullet-},BA)}[SO_4^{\bullet-}]_S\right)t = -k_{(obs,BA}t \tag{2}$$

$$In\frac{[Atrazine]}{[Atrazine]_0} = -k_{(\bullet H,Atrazine)}[\bullet OH] + k_{(SO_4^{\bullet-},Atrazine)}[SO_4^{\bullet-}]_S\ )t = -k_{(obs,Atrazine}t \tag{3}$$

$$[\cdot OH]_s = \frac{\int[\cdot OH]dt}{t} = \frac{k_{(obs,NB)}}{k_{(\cdot OH,NB)}} \tag{4}$$

$$[SO_4^{\bullet-}]_S = \frac{\int[SO_4^{\bullet-}]dt}{t} = \frac{k_{(obs,BA)} - k_{(OH,BA)}[\bullet OH]_s}{k_{(SO_4^{\bullet-},BA)}} \tag{5}$$

$$R_{\cdot OH} = \frac{k_{\cdot OH,Atrazine}[\cdot OH]_s}{k_{obs,Atrazine}} \tag{6}$$

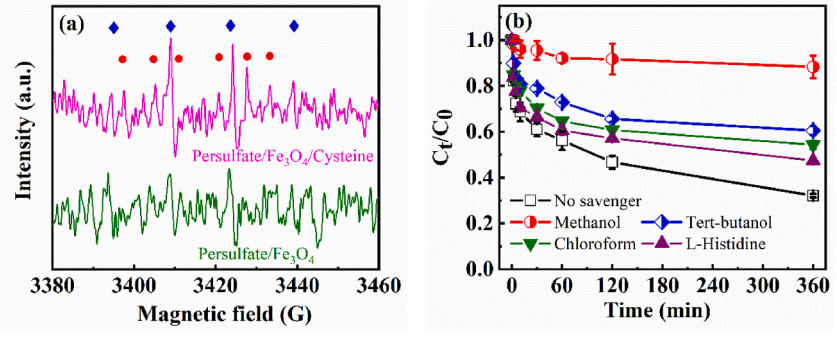

Fig. 2. (A) EPR spectra of Persulfate/Fe_3O_4 and Persulfate/Fe_3O_4/Cysteine at 10 min (● for DMPO-$SO_4^{\bullet-}$, ◆ for DMPO-•OH); (b) Time profiles of the atrazine degradation in Persulfate/Fe_3O_4/Cysteine system with different scavengers (Methanol for scavenger of hydroxyl and sulfate radicals, tert-butanol for scavenger of hydroxyl radicals). The initial condition: [Persulfate] = 1 mmol L^{-1}, [Cysteine] = 0.1 mmol L^{-1}, [Fe_3O_4] = 1 g L^{-1}, [Methanol] = [Tert-butanol] = 100 mmol L^{-1}, the initial pH was 3.0.

$$R_{SO_4^{\cdot-}} = \frac{k_{SO_4^{\cdot-},Atrazine}[SO_4^{\cdot-}]_s}{k_{obs,Atrazine}} \quad (7)$$

$$R_p = 1 - R_{\cdot OH} - R_{SO_4^{\cdot-}} \quad (8)$$

where $[Atrazine]_0$, $[BA]_0$ and $[NB]_0$ were the initial concentration of atrazine, BA and NB, respectively. [Atrazine], [BA]and [NB] represented the concentration of atrazine, BA and NB at t time, respectively. $[\bullet OH]_s$ and $[SO_4^{\bullet-}]_s$ represented the steady-state concentration of $^{\bullet}OH$ and $SO_4^{\bullet-}$, respectively. The $k_{(\bullet OH,\ BA)}$ and $k_{(SO_4^{\bullet-},BA)}$ were the second-order rate constants of BA with $^{\bullet}OH$ and $SO_4^{\bullet-}$, respectively. The $k_{(\bullet OH,\ NB)}$ was the second-order rate constant of NB with $^{\bullet}OH$. The $k_{(\bullet OH,\ Atrazine)}$ and $k_{(SO_4^{\bullet-},Atrazine)}$ were the second-order rate constants of atrazine with $^{\bullet}OH$ and $SO_4^{\bullet-}$, respectively. $R_{\bullet OH}$, $R_{SO4}^{\bullet-}$ and Rp were the relative contribution of $^{\bullet}OH$, $SO_4^{\bullet-}$ and other reactive species, respectively.

3.2. Effect of initial condition on the degradation of atrazine in cysteine/Fe_3O_4/persulfate system

3.2.1. Influences of cysteine, Fe_3O_4 and persulfate concentrations

The influences of different concentrations of cysteine, Fe_3O_4 and persulfate on the degradation efficiency of atrazine were explored to achieve the proper dosages during the process. The impact of the initial cysteine concentration on the removal of atrazine was shown in Fig. 3a. With the increase of the cysteine concentration in range of 0.0–0.2 mmol L^{-1}, the removal ratio of atrazine gradually raised from 28.7 % to 75.4 %. However, the further increase of cysteine addition to 0.5 mmol L^{-1} resulted in the inhibition of atrazine degradation, which might due to the capture of $SO_4^{\bullet-}$ and •OH by the excess cysteine. In our previous study, a similar phenomenon was also observed that the excess ascorbic acid could restrain the degradation of pentachlorophenol by persulfate while the DMPO-$SO_4^{\bullet-}$ peak intensity was significantly weakened [29]. Therefore, the proper dosage of cysteine was set at 0.2 mmol L^{-1}.

Fig. 3b illustrated the impact of Fe_3O_4 concentration on the removal efficiency of atrazine. In the absence of Fe_3O_4, the degradation ratio of atrazine was only 6.7 % after 360 min treatment. As the dosage of Fe_3O_4 increased from 0 g L^{-1} to 1.0 g L^{-1}, the removal ratio of atrazine raised up to 76.8 %, which was owing to the Fe_3O_4 act as a capable provider of Fe^{2+} for the activation of persulfate (Eq. (9)). However, when the addition of Fe_3O_4 was further increased to 2.0 g L^{-1}, the removal ratio of atrazine was not promoted and the degradation rate slightly decreased in the initial 120 min. The excess released Fe^{2+} from Fe_3O_4 had high reduction potential so that it could consume the generated $SO_4^{\bullet-}$ and •OH [35]. Thus, the optimum dosage of Fe_3O_4 was 2.0 g L^{-1}.

$$Fe^{2+} + S_2O_8^{2-} \rightarrow Fe^{3+} + SO_4^{2-} + SO_4^{\cdot-} \quad (9)$$

As shown in Fig. 3c, the effect of persulfate concentration (0–5 mmol L^{-1}) on the oxidation performance of atrazine was

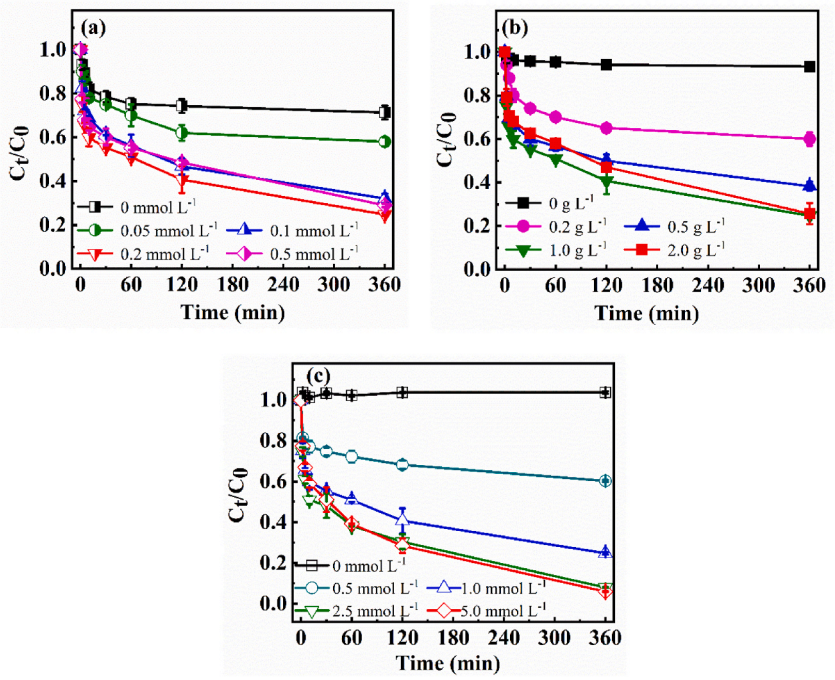

Fig. 3. Decomposition efficiency of atrazine at different concentrations of cysteine (a, the initial condition: [Persulfate] = 1 mmol L^{-1}, [Fe_3O_4] = 1 g L^{-1}), Fe_3O_4 (b, the initial condition: [Persulfate] = 1 mmol L^{-1}, [Cysteine] = 0.2 mmol L^{-1}) and persulfate (c, the initial condition: [Cysteine] = 0.2 mmol L^{-1}, [Fe_3O_4] = 2.0 g L^{-1}). The initial pH was 3.0.

investigated. Without the addition of persulfate, negligible removal of atrazine was observed during the process. When the concentration of persulfate was 0.5 mmol L^{-1}, the removal ratio of atrazine remarkably increased to 40.5 % after 360 min, because persulfate was the necessary driving factor for the generation of $SO_4^{\bullet-}$. The atrazine degradation efficiency showed a positive dependence on persulfate dosage in the range of 0–2.5 mmol L^{-1}. As addition of 2.5 mmol L^{-1} persulfate, the degradation ratio of atrazine achieved 92.1 % after 360 min. Since the sulfate radical could be quenched by $S_2O_8^{2-}$ (Eq. (10)) [36], excess addition of persulfate might result in promotion of sulfate anions yield rather than the production of high active $SO_4^{\bullet-}$. When the concentration of persulfate further increased to 5 mmol L^{-1}, the degradation efficiency of atrazine was not significantly promoted. Hence, the optimal persulfate addition concentration was 2.5 mmol L^{-1}.

$$SO_4^{\cdot-} + S_2O_8^{2-} \rightarrow SO_4^{2-} + S_2O_8^{\cdot-} \quad (10)$$

3.2.2. *Effect of initial pH*

According to previous studies, the pH had a significant impact on the activation of persulfate and the production of reactive radical species [37,38]. To explore the impact of pH on the degradation of atrazine, the initial pH was adjusted to 3.0, 5.0, 7.0, 9.0 and 11.0 respectively. As shown in Fig. 4a, the degradation efficiency of atrazine gradually decreased from 92.1 % to 12.2 % with the solution pH rose from 3.0 to 11.0. The initial pH could affect the surface properties of Fe_3O_4, which indirectly influenced the activation of persulfate. Atrazine molecules (pKa = 1.7) are uncharged in the studied pH (3-11). The Fe_3O_4 surface (pKa = 6.08, Fig. S5 in the SM) was positively charged in the pH range of 3–5 and negatively charged in the pH range of 7–11. Under the pH of 3–5, electrostatic attraction existed between Fe_3O_4 and $S_2O_8^{2-}$ which was beneficial to the activation of persulfate, while electrostatic repulsion between Fe_3O_4 and $S_2O_8^{2-}$ at pH of 7–11 would inhibit the activation of persulfate. Meanwhile, it was reported that the initial pH of the reaction solution might indirectly affect the oxidation of the organic pollutants in the Fe^{2+}/persulfate system through altering the dissociation, speciation and precipitation of iron [39]. Under acidic condition (pH = 3), the dissolved Fe^{2+} was quickly generated and reached 0.34 mmol L^{-1} after 360 min (Fig. S6a in the SM). As the increase of pH, the generation of Fe^{2+} gradually decreased due to the formation of iron hydroxides and further passivation of Fe_3O_4 surface to restrain the release of Fe^{2+}. At pH of 9, the dissolved Fe^{2+} was reduced to 0.012 mmol L^{-1} and negligible dissolved Fe^{2+} was detected under pH of 11 (Fig. S6a in the SM). In addition, the pH strongly influenced the conversion of reactive radical species. $SO_4^{\bullet-}$ could react with OH^- to produce •OH (Eq. (11)) [12]. Fig. 4b showed the EPR spectra of Cysteine/Fe_3O_4/Persulfate system under different pH. As the increase of pH from 3 to 7, the intensity of DMPO-$SO_4^{\bullet-}$ peak was cut down and the peak of DMPO-$SO_4^{\bullet-}$ nearly disappeared at pH 11 which confirmed the conversion of $SO_4^{\bullet-}$ during the process. Quenching experiments were conducted to determine the contribution of $SO_4^{\bullet-}$ and •OH on atrazine degradation under different pH. Table S2 (in the SM) illustrated that $SO_4^{\bullet-}$ was the key radical species under acidic condition, while •OH gradually dominated the oxidation of atrazine from neutral condition to alkaline condition. It was reported that the reaction rate between atrazine and $SO_4^{\bullet-}$ ($k = 4.2 \times 10^9$ M^{-1} S^{-1}) was faster than atrazine and •OH ($k = 2.4–3.0 \times 10^9$ M^{-1} S^{-1}) [3]. In brief, the acidic condition was profit to atrazine degradation by Cysteine/Fe_3O_4/Persulfate treatment. After 360 min reaction, the final pH values were changed to 4.3 , 4.7, 5.2, 7.3 and 8.9, respectively (Fig. S6b in the SM). When the initial pH values were 3.0 and 5.0, the pH increased along the reaction, owing to the consumption of H^+ by Fe_3O_4 dissolution (Eq (12)). At neutral and alkaline condition, the pH values were reduced at the initial stage, which might be due to the hydrolysis of persulfate (Eq. (13) and (14)) and the consumption of OH^- (Eq (11)).

$$SO_4^{\cdot-} + OH^- \rightarrow SO_4^{2-} + \cdot OH \quad (11)$$

$$Fe_3O_4 + 8H^+ \rightarrow Fe^{2+} + 2Fe^{3+} + 4H_2O \quad (12)$$

$$S_2O_8^{2-} + 2H_2O \rightarrow 2SO_4^{2-} + HO_2^- + 3H^+ \quad (13)$$

$$2S_2O_8^{2-} + 2H_2O \rightarrow 4SO_4^{2-} + O_2 + 4H^+ \quad (14)$$

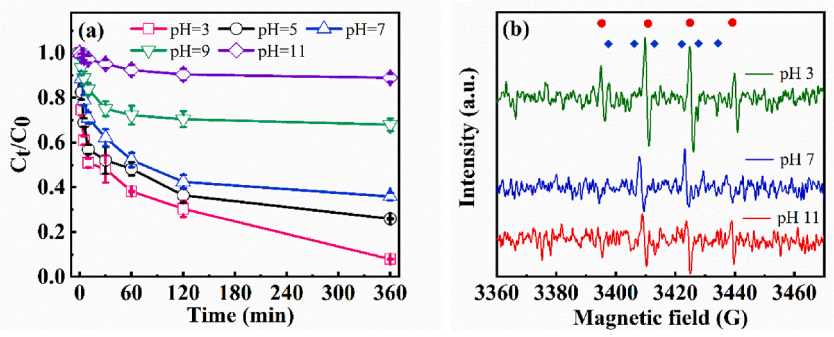

Fig. 4. (A) Degradation efficiency of atrazine and (b) the intensity of DMPO-$SO_4^{\bullet-}$ (◆) and DMPO-•OH (●) in different initial pH. The initial condition: [Persulfate] = 2.5 mmol L^{-1}, [Cysteine] = 0.2 mmol L^{-1}, [Fe_3O_4] = 2 g L^{-1}.

3.2.3. Influence of co-existing inorganic ions and natural organic matters

In actual polluted water, atrazine often coexists with inorganic ions and natural organic matter (NOM). The effect of co-existing inorganic ions and NOM on the degradation efficiency of atrazine by Cysteine/Fe_3O_4/Persulfate system was shown in Fig. 5. Negligible impact on atrazine removal was observed with different addition of NO_3^-, while the removal ratio of atrazine significantly reduced as the increase of Cl^- and HCO_3^- concentrations in the range of 0–20 mmol L^{-1} (Fig. 5a). The intensity of DMPO-$SO_4^{\bullet-}$ maintained stable in the presence of different dosage of NO_3^- (Fig. S7 in the SM), indicating that NO_3^- could not efficiently quenching sulfate radicals. However, the intensities of DMPO-$SO_4^{\bullet-}$ were obviously cut down with addition of various Cl^- and HCO_3^- dosages (Fig. S7 in the SM), confirming that Cl^- and HCO_3^- can capture sulfate radicals. Cl^- reacted with sulfate radicals to produce $Cl^{\bullet}$, $Cl_2^{\bullet-}$ and Cl_2 (Eq. (15)–(17)). The oxidation potential of $Cl^{\bullet}$ ($E_0 = 2.4$ V), $Cl_2^{\bullet-}$ ($E_0 = 2.1$ V) and Cl_2 ($E_0 = 1.4$ V) were lower than $SO_4^{\bullet-}$ ($E_0 =$ 2.5–3.1 V) [40], so that the degradation of atrazine was restrained after the conversion of sulfate radical to chlorine species. The HCO_3^- can also react with sulfate radicals to generate $CO_3^{\bullet-}$ (Eq. (18)) [41,42]. The oxidation potential of $CO_3^{\bullet-}$ ($E_0 = 1.78$ V) is much less than $Cl^{\bullet}$, $Cl_2^{\bullet-}$ and $SO_4^{\bullet-}$, resulting in a stronger negative effect on atrazine degradation with addition of HCO_3^- than Cl^-.

$$SO_4^{\cdot-} + Cl^- \rightarrow SO_4^{2-} + Cl^{\cdot} \quad (15)$$

$$Cl^{\cdot} + Cl^- \rightarrow Cl_2^{\cdot-} \quad (16)$$

$$2Cl_2^{\cdot-} \rightarrow 2Cl^- + Cl_2 \quad (17)$$

$$SO_4^{\cdot-} + HCO_3^- \rightarrow SO_4^{2-} + H + CO_3^{\cdot-} \quad (18)$$

As shown in Fig. 5b, a significant enhancement on atrazine degradation was observed in the presence of low NOM concentration (0–2 mg L^{-1}). This might be owing to the quinone functional groups in NOM could form semiquinone radical ($SQ^{\bullet-}$) which subsequently activate persulfate to generate $SO_4^{\bullet-}$ (Eq. (19)) [15]. However, as further increasing of NOM concentration to 5 mg L^{-1} and 10 mg L^{-1}, the removal ratio of atrazine reduced to 80.2 % and 67.1 %, respectively. It was ascribed to the competitive consumption of the generated $SO_4^{\bullet-}$ between the excess NOM and atrazine.

$$SQ^{\cdot-} + S_2O_8^{2-} \rightarrow SO_4^{\cdot-} + Q \quad (19)$$

3.2.4. Estimation the performance of cysteine/Fe_3O_4/persulfate system on the degradation of atrazine

After investigating the influence factors on the degradation of atrazine in Cysteine/Fe_3O_4/Persulfate system, we obtained the optimum dosage of persulfate, cysteine and Fe_3O_4. The removal ratio of atrazine reached 92.1 % with 2.5 mmol L^{-1} persulfate, 0.2 mmol L^{-1} cysteine and 2.0 g L^{-1} Fe_3O_4 after 360 min. Since the structure of atrazine is very stable, it is difficult to be degraded. Compared to the other systems reported in the latest references (Table S3 in the SM), our system in the current study showed a better performance on the removal of atrazine than ozonation, electrochemical oxidation, Fenton-like system and photo-electrochemical oxidation. In addition, the system was not dependent on energy consumption and the required materials was economical and environmental-friendly, which could reflect the advantages of the system.

3.3. The role of Fe_3O_4 and cysteine in cysteine/Fe_3O_4/persulfate system

Fig. S8 (in the SM) showed the characterization of Fe_3O_4 before and after the reaction by SEM, NSP and XRD. The SEM images showed Fe_3O_4 had porous surface structure which supplied more sites to activate persulfate. After the oxidation process, Fe_3O_4 was obviously corroded and its surface has become rough (Fig. S8a in the SM). According to the particle size distribution, the average particle size of Fe_3O_4 was significantly reduced after the treatment (Fig. S8b in the SM). Meanwhile, negligible changes were observed in the XRD patterns of Fe_3O_4 after the reaction (Fig. S8c in the SM), which indicated structure of the Fe_3O_4 was reasonably steady during the process. Fe_3O_4 can release Fe^{2+} and Fe^{3+} by reaction with H^+ (Eq (4)) and cysteine (Fig. S9 in the SM), including dissolved

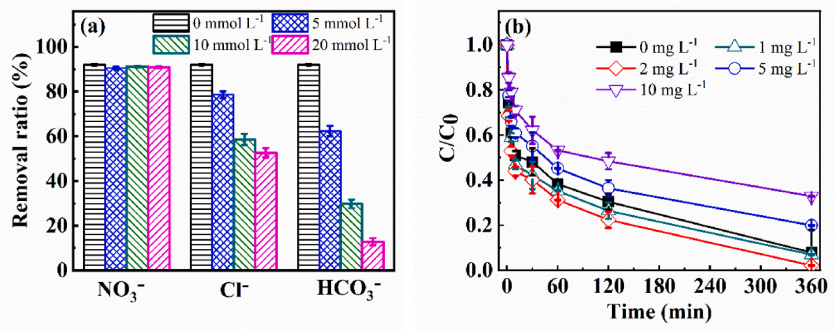

Fig. 5. The effect of inorganic ions (a) and NOM (b) on the degradation efficiency of atrazine by Cysteine/Fe_3O_4/Persulfate system. The initial condition: [Persulfate] = 2.5 mmol L^{-1}, [Cysteine] = 0.2 mmol L^{-1}, [Fe_3O_4] = 2 g L^{-1}, the initial pH was 3.0.

and surface bound states. It has been reported that Fe^{2+} could directly activate persulfate by single electron transfer (Eq (1)). To explore the contribution of Fe^{2+} on the persulfate activation during Cysteine/Fe_3O_4/Persulfate process, excess 2,2-bipyridine (BPY) was employed to complex with Fe^{2+} for prohibiting its oxidation with persulfate [43]. Fig. 6a illustrated that the addition of BPY could completely suppress the degradation of atrazine by Cysteine/Fe_3O_4/Persulfate system. Since the concentration of BPY remained unchanged during the process (Fig. S10 in the SM), the consumption of persulfate by BPY could be excluded. Therefore, Fe^{2+} played a key role on the activation of persulfate. Subsequently, we compared the degradation efficiencies of atrazine in Cysteine/Fe_3O_4/Persulfate and Cysteine/Fe^{2+}/Persulfate system with Fe^{2+} of 0.34 mmol L^{-1} (the highest concentration of dissolved Fe^{2+} in the Cysteine/Fe_3O_4/Persulfate system) under the same condition. It showed that only 33.2 % of atrazine was removed after 360 min in the Cysteine/Fe^{2+}/Persulfate system, which was much lower than Cysteine/Fe_3O_4/Persulfate system (92.1 %), suggesting indispensable contribution of surface bound Fe^{2+} on the activation of persulfate for atrazine degradation.

Cysteine has a carboxyl group (-COOH) so that it can enhance the release of iron ions from Fe_3O_4 by complexation. To confirm this process, we monitored the dissolved Fe^{2+}, Fe^{3+} and total Fe concentrations in the Cysteine/Fe_3O_4/Persulfate system and Fe_3O_4/Persulfate system. It could be observed that the dissolved total Fe concentrations in the Cysteine/Fe_3O_4/Persulfate system were much higher than that in Fe_3O_4/Persulfate system at the same condition (Fig. 7a). The result indicated that the addition of cysteine could significantly promote the release of iron ions from Fe_3O_4, which was beneficial for enhancing persulfate activation. Besides complexation, cysteine has a thiol group (-SH), which can act as a reductant to reduce Fe^{3+} to Fe^{2+}. In theory, Fe_3O_4 simultaneously released Fe^{2+} and Fe^{3+} by acidolysis or complexation. However, negligible Fe^{3+} was detected in the initial 15 min during the Cysteine/Fe_3O_4/Persulfate process (Fig. 7a), which might be owing to the enough cysteine quickly reduced the generated Fe^{3+} to Fe^{2+} in this stage. To further verify this opinion, 0.1 mol L^{-1} $AgNO_3$ was added at 60 min during the process, which could quench the thiol group in cysteine. It could be observed that the dissolved Fe^{2+} could not keep increasing after the addition of $AgNO_3$, while the accumulation of Fe^{3+} obviously improved (Fig. S11 in the SM), suggesting the cycle of Fe^{2+} and Fe^{3+} was dependent on the presence of cysteine. As an organic compounds, cysteine might be oxidized by ROSs during the Cysteine/Fe_3O_4/Persulfate process, resulting in the unsustainable Fe^{2+}/Fe^{3+} cycle. It had been reported that ascorbic acid could accelerate the cycle of Fe^{2+}/Fe^{3+} to promote the degradation of organic contaminants by a Fenton-like system [44]. However, ascorbic acid was exhausted after 20 min reaction, accompanying with dissolved Fe^{2+} concentration quickly decreased. Fortunately, cysteine was not rapidly consumed, and the retention ratios of cysteine were 70.6 % and 52.4 % at 60 min and 360 min respectively (Fig. 7b). At the same time, cystine was detected and its concentration increased in the initial 30 min and then slowly decreased. The generation of cystine might be dS2erived from the combination of cysteine radical ((Eq. (20) and (21)), followed by the reproduction of cysteine through the reaction between cystine and •OH [26]. The stable presence of cysteine was beneficial for maintaining the Fe^{2+}/Fe^{3+} cycle and the concentration of Fe^{2+} continued to increase during the process (Fig. S6a in the SM), which constantly accelerate the activation of persulfate for atrazine degradation. Hence, the oxidation of atrazine nearly stagnated after 60 min in the Fe_3O_4/Persulfate system, while atrazine still maintained a high degradation rate in Cysteine/Fe_3O_4/Persulfate system (Fig. 1a).

$$[\mathrm{Fe(Cysteine)}]^{2+} \rightarrow \mathrm{Fe}^{2+} + \mathrm{Cysteine}^{\cdot} \tag{20}$$

$$2\mathrm{Cysteine}^{\cdot} \rightarrow \mathrm{Cystine} \tag{21}$$

Since Fe_3O_4 and cysteine were stable during the Cysteine/Fe_3O_4/Persulfate process. Reusability of Fe_3O_4 and cysteine was tested by three cycles with the concentrations of atrazine and persulfate were recovered to the initial stage before each cycle. The reused Fe_3O_4 and cysteine in the Cysteine/Fe_3O_4/Persulfate process exhibited high activity for the degradation of atrazine. The removal ratios of atrazine were achieved 92.1 % and 85.3 % after the first and second cycle respectively (Fig. S12 in the SM). As the consumption of cysteine, the generation of Fe^{2+} was inhibited, resulting in the removal ratios of atrazine reduced to 59.7 % after the third cycle.

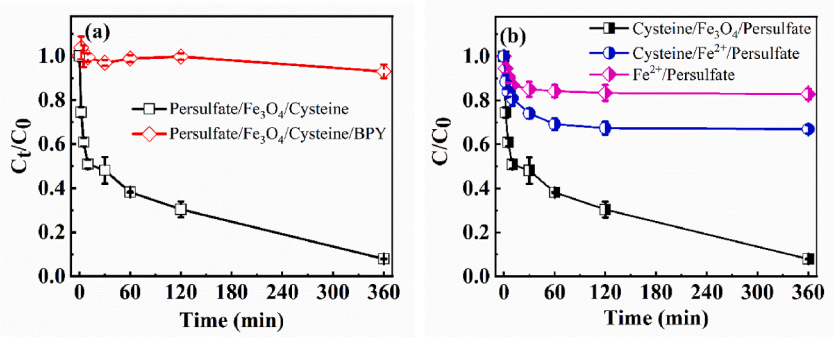

Fig. 6. (A) The influence of BPY on the degradation of atrazine by Cysteine/Fe_3O_4/Persulfate system; (b) Time profiles of atrazine degradation in the Cysteine/Fe_3O_4/Persulfate, Cysteine/Fe^{2+}/Persulfate and Fe^{2+}/Persulfate systems. The initial condition: [Persulfate] = 2.5 mmol L^{-1}, [Cysteine] = 0.2 mmol L^{-1}, [Fe^{2+}] = 0.34 mmol L^{-1}, [Fe_3O_4] = 2 g L^{-1}, [BPY] = 50 mmol L^{-1}, the initial pH was 3.0.

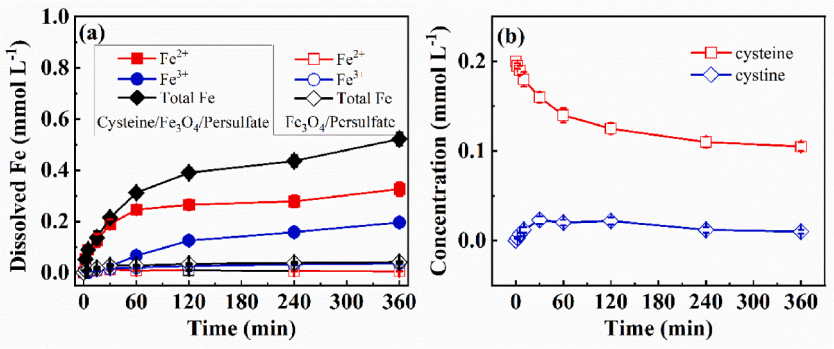

Fig. 7. (A) Variation of Fe^{2+}, Fe^{3+} and total Fe concentrations in the Cysteine/Fe_3O_4/Persulfate system and Fe_3O_4/Persulfate system; (b) Time profiles of cysteine and cystine concentration in the Cysteine/Fe_3O_4/Persulfate system. The initial condition: [Persulfate] = 2.5 mmol L^{-1}, [Cysteine] = 0.2 mmol L^{-1}, [Fe_3O_4] = 2 g L^{-1}, the initial pH was 3.0.

3.4. Proposed pathways of atrazine degradation in the cysteine/Fe_3O_4/persulfate system

TOC analysis was used to determine the mineralization performance of atrazine. Although 72.3 % of atrazine was degraded by Cysteine/Fe_3O_4/Persulfate system, the removal ratio of TOC was only 30.6 % after 360 min (Fig. S13 in the SM), indicating that atrazine would break down into smaller molecules and undergo partial mineralization during the process. The identification of intermediates is beneficial to further reveal the degradation mechanism of atrazine in the Cysteine/Fe_3O_4/Persulfate system. The intermediates were detected by LC-MS analysis (Fig. S14 in the SM), containing 2-chloro-4-amino-6-isopropylamine-1,3,5-triazine (CAIT, *m/z* 188.0710), 2-hydroxy-6-isopropylamine-1,3,5-triazine (HEA, *m/z* 114.0927), 1-(4-chloro-6-(isopropylamino)-1,3,5-triazin-2-ylamino) ethanol (CNIT, *m/z* 232.0784), 2-chloro-4-acetylamino-6-isopropylamine-1,3,5-triazine (CDIT, *m/z* 230.0817), N-(4-hydroxy-6-isopropylamine)-1,3,5-trazine-2-acetamide (ODIT, *m/z* 212.1147) and 2-hydroxy-4-ethylamine-6-isopropylamine-1,3,5-triazine (HYA, *m/z* 198.1354). Based on the intermediates and ROSs that had been identified, we could propose a possible degradation pathway of atrazine in the Cysteine/Fe_3O_4/Persulfate system, including alkylic-oxidation, dealkylation, dechlorination-hydroxylation processes (Fig. 8). Generally, atrazine could quickly react with ROSs by H-abstraction at the lateral chains due to the lack of double bond [45]. As the C–H in the lateral chain of atrazine was attacked by •OH, alkylic hydroxylation products (CNIT) was formed. Meanwhile, the fracture of C–C and C–N bonds in the lateral chain of atrazine induced the generation of dealkylation products (CAIT). Due to the longest bond length and relatively low bond polarity, the C–Cl bond in atrazine was effortless to be broken down by oxidation with ROSs [46], leading to the formation of dechlorination-hydroxylation products (HYA). Chloride ions had been detected in the solution (Fig. 1b), which further confirmed the occurrence of dechlorination behavior during the process. CNIT was unstable and it could be easily oxidized by $SO_4^{\bullet-}$ and •OH to generate CDIT [47]. Subsequently, CDIT could be oxidized by ROSs through dechlorination-hydroxylation process to generate ODIT. The oxidation process further induced the cleavage of C–N and C–C bonds in the lateral chain of ODIT to form HEA.

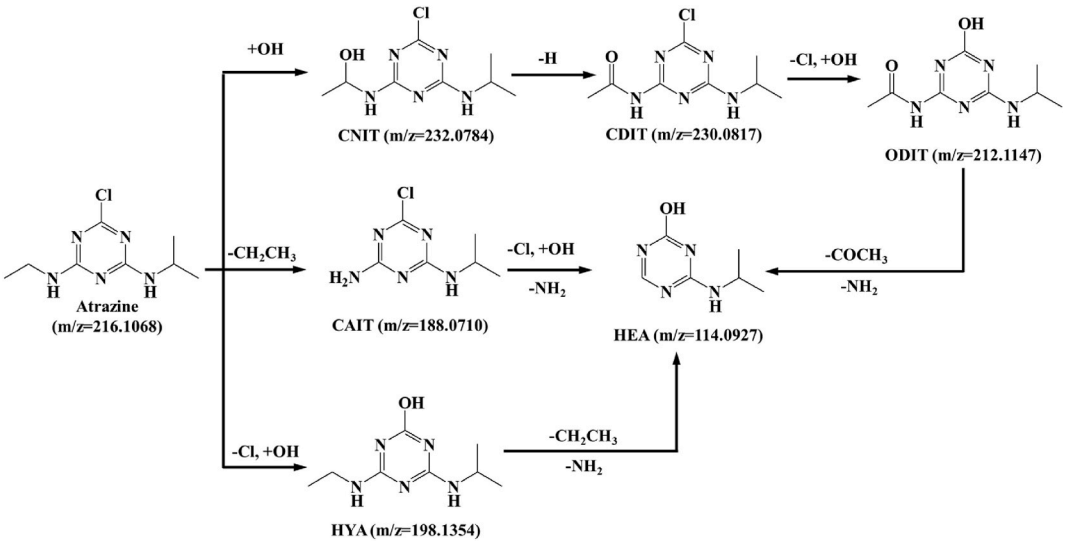

Fig. 8. The possible degradation pathways of atrazine in Cysteine/Fe_3O_4/Persulfate system.

4. Conclusions

In this study, we interestingly discovered the presence of cysteine could significantly enhance the degradation of atrazine by Fe_3O_4/persulfate system. As a type of necessary amino acid, cysteine is environmentally benign and pervasively found in many living cells of organisms, so that it is economical and safe for treatment of environment pollution. According to EPR spectra analysis, the combination of cysteine and Fe_3O_4 could induce activation of persulfate to generate more $SO_4^{\bullet-}$ and •OH than Fe_3O_4 alone. The degradation efficiency of atrazine was dependent on suitable dosage of chemical reagent (cysteine, Fe_3O_4 and persulfate) and pH condition. The co-existing inorganic ions and natural organic matters also effected the atrazine degradation. Cysteine played two key roles during the process: (i) enhancing release of dissolved and surface bound Fe^{2+} from Fe_3O_4; (ii) maintaining Fe^{2+}/Fe^{3+} cycle to constantly accelerate the activation of persulfate. In addition, cysteine could be regenerated during the process, so that it could be reused in the practical application with low cost. These findings may point to a viable alternative for the treatment of organic polluted water by Cysteine/Fe_3O_4/Persulfate system.

CRediT authorship contribution statement

Mingming Zheng: Investigation, Writing - original draft. **Yinghao Li:** Data curation, Investigation, Writing - original draft. **Menghua Cao:** Funding acquisition, Project administration, Writing - review & editing. **Yuxin Guo:** Formal analysis, Investigation. **Guohong Qiu:** Writing - review & editing. **Shuxin Tu:** Writing - review & editing. **Shuanglian Xiong:** Writing - review & editing. **Dun Fang:** Data curation, Investigation.

Declaration of competing interest

The authors declare that they have no known competing financial interests or personal relationships that could have appeared to influence the work reported in this paper.

Acknowledgements

This work was supported by National Natural Science Foundation of China (Grant 21976065), Natural Science Foundation of Hubei Province (Grant 2022CFD003 and Grant 2023AFD066) and Wuhan Project on Knowledge Innovation (Grant 2022020801020398).

Appendix A. Supplementary data

Supplementary data to this article can be found online at https://doi.org/10.1016/j.heliyon.2023.e23371.

References

[1] A. Iriel, J.M. Novo, G.B. Cordon, M.G. Lagorio, Atrazine and methyl viologen effects on chlorophyll-a fluorescence revisited-implications in photosystems emission and ecotoxicity assessment, Photochem. Photobiol. 90 (2014) 107–112, https://doi.org/10.1111/php.12142.
[2] A. Kumar, N. Singh, Atrazine and its metabolites degradation in mineral salts medium and soil using an enrichment culture, Environ. Monit. Assess. 188 (2016) 142, https://doi.org/10.1007/s10661-016-5144-3.
[3] Y.H. Guan, J. Ma, Y.M. Ren, Y.L. Liu, J.Y. Xiao, L.Q. Lin, C. Zhang, Efficient degradation of atrazine by magnetic porous copper ferrite catalyzed peroxymonosulfate oxidation via the formation of hydroxyl and sulfate radicals, Water Res. 47 (2013) 5431–5438, https://doi.org/10.1016/j.watres.2013.06.023.
[4] S. Singh, V. Kumar, A. Chauhan, S. Datta, A.B. Wani, N. Singh, J. Singh, Toxicity, degradation and analysis of the herbicide atrazine, Environ. Chem. Lett. 16 (2018) 211–237, https://doi.org/10.1007/s10311-017-0665-8.
[5] J. Bethsass, A. Colangelo, European Union bans atrazine, while the United States negotiates continued use, Int. J. Occup. Environ. Heal. 12 (2006) 260–267, https://doi.org/10.1179/oeh.2006.12.3.260.
[6] H.S. Ahn, T.D. Tilley, Electrocatalytic water oxidation at neutral pH by a nanostructured $Co(PO_3)_2$ anode, Adv. Funct. Mater. 23 (2013) 227–233, https://doi.org/10.1002/adfm.201200920.
[7] S. Wacławek, H.V. Lutze, K. Grübel, V.V.T. Padil, M. Černík, D.D. Dionysiou, Chemistry of persulfates in water and wastewater treatment: a review, Chem. Eng. J. 330 (2017) 44–62, https://doi.org/10.1016/j.cej.2017.07.132.
[8] B.C. Hodges, E.L. Cates, J.H. Kim, Challenges and prospects of advanced oxidation water treatment processes using catalytic nanomaterials, Nature Nanotech 13 (2018) 642–650, https://doi.org/10.1038/s41565-018-0216-x.
[9] J.L. Wang, S.Z. Wang, Activation of persulfate (PS) and peroxymonosulfate (PMS) and application for the degradation of emerging contaminants, Chem. Eng. J. 334 (2018) 1502–1517, https://doi.org/10.1016/j.cej.2017.11.059.
[10] Y. Qian, X. Guo, Y. Zhang, Y. Peng, P. Sun, C.H. Huang, J. Niu, X. Zhou, J.C. Crittenden, Perfluorooctanoic acid degradation using UV-persulfate process: modeling of the degradation and chlorate formation, Environ. Sci. Technol. 50 (2016) 772–781, https://doi.org/10.1021/acs.est.5b03715.
[11] G.D. Fang, D.D. Dionysiou, D.M. Zhou, Y. Wang, X.D. Zhu, J.X. Fan, L. Cang, Y.J. Wang, Transformation of polychlorinated biphenyls by persulfate at ambient temperature, Chemosphere 90 (2013) 1573–1580, https://doi.org/10.1016/j.chemosphere.2012.07.047.
[12] O.S. Furman, A.L. Teel, R.J. Watts, Mechanism of base activation of persulfate, Environ. Sci. Technol. 44 (2010) 6423–6428, https://doi.org/10.1021/es1013714.
[13] J.Y. Zhao, Y.B. Zhang, X. Quan, S. Chen, Enhanced oxidation of 4-chlorophenol using sulfate radicals generated from zero-valent iron and peroxydisulfate at ambient temperature, Sep. Purif. Technol. 71 (2010) 302–307, https://doi.org/10.1016/j.seppur.2009.12.010.
[14] J. Chen, L. Zhang, T. Huang, W. Li, Y. Wang, Z. Wang, Decolorization of azo dye by peroxymonosulfate activated by carbon nanotube: radical versus non-radical mechanism, J. Hazard Mater. 320 (2016) 571–580, https://doi.org/10.1016/j.jhazmat.2016.07.038.

[15] G.D. Fang, J. Gao, D.D. Dionysiou, C. Liu, D.M. Zhou, Activation of persulfate by quinones: free radical reactions and implication for the degradation of PCBs, Environ. Sci. Technol. 47 (2013) 4605–4611, https://doi.org/10.1021/es400262n.

[16] S. Wang, J. Wang, Trimethoprim degradation by Fenton and Fe(II)-activated persulfate processes, Chemosphere 191 (2018) 97–105, https://doi.org/10.1016/j.chemosphere.2017.10.040.

[17] D. Han, J. Wan, Y. Ma, Y. Wang, Y. Li, D. Li, Z. Guan, New insights into the role of organic chelating agents in Fe(II) activated persulfate processes, Chem. Eng. J. 269 (2015) 425–433, https://doi.org/10.1016/j.cej.2015.01.106.

[18] S. Yan, X. Zhang, H. Zhang, Persulfate activation by Fe(III) with bioelectricity at acidic and near-neutral pH regimes: Homogeneous versus heterogeneous mechanism, J. Hazard Mater. 374 (2019) 92–100, https://doi.org/10.1016/j.jhazmat.2019.03.068.

[19] Y. Li, F. Wang, X. Ren, P. Wang, F.X. Wang, H.-Y. Chu, S. Gao, C.C. Wang, Peroxymonosulfate activation for effective atrazine degradation over a 3D cobalt-MOF: performance and mechanism, J. Environ. Chem. Eng. 11 (2023), 109116, https://doi.org/10.1016/j.jece.2022.109116.

[20] F. Wang, S.S. Liu, Z. Feng, H. Fu, M. Wang, P. Wang, W. Liu, C.C. Wang, High-efficient peroxymonosulfate activation for rapid atrazine degradation by FeSx@MoS2 derived from MIL-88A(Fe), J. Hazard Mater. 440 (2022), 129723, https://doi.org/10.1016/j.jhazmat.2022.129723.

[21] A. Rastogi, S.R. Al-Abed, D.D. Dionysiou, Effect of inorganic, synthetic and naturally occurring chelating agents on Fe(II) mediated advanced oxidation of chlorophenols, Water Res. 43 (2009) 684–694, https://doi.org/10.1016/j.watres.2008.10.045.

[22] L. Zhou, W. Zheng, Y. Ji, J. Zhang, C. Zeng, Y. Zhang, Q. Wang, X. Yang, Ferrous-activated persulfate oxidation of arsenic(III) and diuron in aquatic system, J. Hazard Mater. 263 (2013) 422–430, https://doi.org/10.1016/j.jhazmat.2013.09.056.

[23] S. Yuan, P. Liao, A.N. Alshawabkeh, Electrolytic manipulation of persulfate reactivity by iron electrodes for trichloroethylene degradation in groundwater, Environ. Sci. Technol. 48 (2014) 656–663, https://doi.org/10.1021/es404535q.

[24] R. Yin, L. Hu, D. Xia, J. Yang, C. He, Y. Liao, Q. Zhang, J. He, Hydroxylamine promoted Fe(III)/Fe(II) cycle on ilmenite surface to enhance persulfate catalytic activation and aqueous pharmaceutical ibuprofen degradation, Cata. Today 358 (2020) 294–302, https://doi.org/10.1016/j.cattod.2019.04.081.

[25] G. Salemi, M.C. Gueli, M. D'Amelio, V. Saia, P. Mangiapane, P. Aridon, P. Ragonese, I. Lupo, Blood levels of homocysteine, cysteine, glutathione, folic acid, and vitamin B12 in the acute phase of atherothrombotic stroke, Neurol. Sci. 30 (2009) 361–364, https://doi.org/10.1007/s10072-009-0090-2.

[26] T. Li, Z. Zhao, Q. Wang, P. Xie, J. Ma, Strongly enhanced Fenton degradation of organic pollutants by cysteine: an aliphatic amino acid accelerator outweighs hydroquinone analogues, Water Res. 105 (2016) 479–486, https://doi.org/10.1016/j.watres.2016.09.019.

[27] R. Doong, B. Schink, Cysteine-Mediated reductive dissolution of poorly Crystalline iron(III) oxides by geobacter sulfurreducens, Environ. Sci. Technol. 36 (2002) 2939–2945, https://doi.org/10.1021/es0102235.

[28] F. Jiang, Y. Li, W. Zhou, Z. Yang, Y. Ning, D. Liu, Z. Tang, S. Yang, H. Huang, G. Wang, Enhanced degradation of monochlorobenzene in groundwater by ferrous iron/persulfate process with cysteine, Chem. Eng. J. 387 (2020), 124048, https://doi.org/10.1016/j.cej.2020.124048.

[29] M. Cao, Y. Hou, E. Zhang, S. Tu, S. Xiong, Ascorbic acid induced activation of persulfate for pentachlorophenol degradation, Chemosphere 229 (2019) 200–205, https://doi.org/10.1016/j.chemosphere.2019.04.135.

[30] C.J. Liang, C.F. Huang, N. Mohanty, R.M. Kurakalva, A rapid spectrophotometric determination of persulfate anion in ISCO, Chemosphere 73 (2008) 1540–1543, https://doi.org/10.1016/j.chemosphere.2008.08.043.

[31] Y. Zhang, B. Zhang, Y. Teng, J. Zhao, X. Sun, Heterogeneous activation of persulfate by carbon nanofiber supported Fe_3O_4@carbon composites for efficient ibuprofen degradation, J. Hazard Mater. 401 (2021), 123428, https://doi.org/10.1016/j.jhazmat.2020.123428.

[32] G. Wu, Y. Katsumura, G. Chu, Photolytic and radiolytic studies of $SO_4^{\bullet-}$ in neat organic solvents, Phys. Chem. Chem. Phys. 2 (2000) 5602–5605, https://doi.org/10.1039/B007274P.

[33] Z.C. Zhang, F.X. Wang, F. Wang, C.C. Wang, P. Wang, Efficient atrazine degradation via photoactivated SR-AOP over S-BUC-21(Fe): the formation and contribution of different reactive oxygen species, Sep. Purif. Technol. 307 (2023), 122864, https://doi.org/10.1016/j.seppur.2022.122864.

[34] J. Liang, X. Duan, X. Xu, K. Chen, Y. Zhang, L. Zhao, H. Qiu, S. Wang, X. Cao, Persulfate oxidation of sulfamethoxazole by magnetic iron-char composites via nonradical pathways: Fe(IV) versus surface-mediated electron transfer, Environ. Sci. Technol. 55 (2021) 10077–10086, https://doi.org/10.1021/acs.est.1c01618.

[35] Y. Leng, W. Guo, X. Shi, Y. Li, L. Xing, Polyhydroquinone-coated Fe_3O_4 nanocatalyst for degradation of rhodamine B based on sulfate radicals, Ind. Eng. Chem. Res. 52 (2013) 13607–13612, https://doi.org/10.1021/ie4015777.

[36] X. Wei, N. Gao, C. Li, Y. Deng, S. Zhou, L. Li, Zero-valent iron (ZVI) activation of persulfate (PS) for oxidation of bentazon in water, Chem. Eng. J. 285 (2016) 660–670, https://doi.org/10.1016/j.cej.2015.08.120.

[37] Z. Dong, C. Jiang, J. Yang, X. Zhang, W. Dai, P. Cai, Transformation of iodide by Fe(II) activated peroxydisulfate, J. Hazard Mater. 373 (2019) 519–526, https://doi.org/10.1016/j.jhazmat.2019.03.063.

[38] M. Ahmad, A.L. Teel, R.J. Watts, Mechanism of persulfate activation by phenols, Environ. Sci. Technol. 47 (2013) 5864–5871, https://doi.org/10.1021/es400728c.

[39] A. Rastogi, S.R. Al-Abed, D.D. Dionysiou, Sulfate radical-based ferrous-peroxymonosulfate oxidative system for PCBs degradation in aqueous and sediment systems, Appl. Catal. B Environ. 85 (2009) 171–179, https://doi.org/10.1016/j.apcatb.2008.07.010.

[40] H. Chen, Z. Zhang, M. Feng, W. Liu, W. Wang, Q. Yang, Y. Hu, Degradation of 2,4-dichlorophenoxyacetic acid in water by persulfate activated with FeS (mackinawite), Chem. Eng. J. 313 (2017) 498–507, https://doi.org/10.1016/j.cej.2016.12.075.

[41] J. Peng, X. Lu, X. Jiang, Y. Zhang, Q. Chen, B. Lai, G. Yao, Degradation of atrazine by persulfate activation with copper sulfide (CuS): kinetics study, degradation pathways and mechanism, Chem. Eng. J. 354 (2018) 740–752, https://doi.org/10.1016/j.cej.2018.08.038.

[42] M.L. Dell'Arciprete, J.M. Soler, L. Santos-Juanes, A. Arques, D.O. Mártire, J.P. Furlong, M.C. Gonzalez, Reactivity of neonicotinoid insecticides with carbonate radicals, Water Res. 46 (2012) 3479–3489, https://doi.org/10.1016/j.watres.2012.03.051.

[43] W. Liu, Z. Ai, M. Cao, L. Zhang, Ferrous ions promoted aerobic simazine degradation with Fe@Fe2O3 core–shell nanowires, Appl. Catal. B Environ. 150–151 (2014) 1–11, https://doi.org/10.1016/j.apcatb.2013.11.034.

[44] H. Sun, G. Xie, D. He, L. Zhang, Ascorbic acid promoted magnetite Fenton degradation of alachlor: mechanistic insights and kinetic modeling, Appl. Cata. B: Environ. 267 (2020), 118383, https://doi.org/10.1016/j.apcatb.2019.118383.

[45] J.A. Khan, X. He, N.S. Shah, H.M. Khan, E. Hapeshi, D. Fatta-Kassinos, D.D. Dionysiou, Kinetic and mechanism investigation on the photochemical degradation of atrazine with activated H_2O_2, $S_2O_8^{2-}$ and HSO_5^-, Chem. Eng. J. 252 (2014) 393–403, https://doi.org/10.1016/j.cej.2014.04.104.

[46] C. Chen, S. Yang, Y. Guo, C. Sun, C. Gu, B. Xu, Photolytic destruction of endocrine disruptor atrazine in aqueous solution under UV irradiation: products and pathways, J. Hazard Mater. 172 (2009) 675–684, https://doi.org/10.1016/j.jhazmat.2009.07.050.

[47] S. Wu, H. He, X. Li, C. Yang, G. Zeng, B. Wu, S. He, L. Lu, Insights into atrazine degradation by persulfate activation using composite of nanoscale zero-valent iron and graphene: performances and mechanisms, Chem. Eng. J. 341 (2018) 126–136, https://doi.org/10.1016/j.cej.2018.01.136.